Title Page

Title:

A curve fitting approach to estimate the arterial plasma input function for estimation of the glucose metabolic rate and response to treatment

Foot Line:

Fitted Input Function to Estimate MR_{glc}

Authors:

Dennis Vriens, Lioe-Fee de Geus-Oei, Wim J.G. Oyen, Eric. P. Visser

Affiliations:

Department of Nuclear Medicine

Radboud University Nijmegen Medical Center

Nijmegen, the Netherlands

Correspondence:

Dennis Vriens

Radboud University Nijmegen Medical Center, department of Nuclear Medicine 444

P.O. Box 9101, 6500 HB Nijmegen, the Netherlands

Tel: +31-24-3665047; Fax: +31-24-3618942; E-Mail: D.Vriens@nucmed.umcn.nl

Word count whole document:

4677

Abstract

Rationale: For quantification of dynamic [^{18}F]-2-fluoro-2-deoxy-D-glucose (^{18}F-FDG) PET studies, the arterial plasma time activity concentration curve (APTAC) needs to be available. This can be obtained by serial arterial blood sampling or by using an image derived input function (IDIF). Arterial sampling is invasive and often not feasible in practice; IDIF's are biased due to partial volume effects and cannot be used when no large arterial blood pool is in the field of view. We propose a mathematical function to describe the APTAC, consisting of initial linear rising activity concentration followed by a tri-exponential decay. This function was fitted to 80 oncological patients and verified for 40 different oncological patients by comparing areas under the curves, Patlak glucose metabolic rate (MR_{glc}) estimation and therapy response monitoring (ΔMR_{glc}). The proposed function was compared with the gold standard (serial arterial sampling) and the IDIF. **Materials and Methods:** To determine the free parameters of the function, plasma time activity curves based on arterial samples in 80 patients were fitted after normalization for administered activity (AA) and initial distribution volume (iDV) of ^{18}F-FDG. The medians of these free parameters were used for the model. In 40 other patients (20 baseline and 20 follow-up dynamic ^{18}F-FDG-PET scans) this model was validated. The population-based curve, individually calibrated by AA and iDV ($APTAC_{AA/iDV}$), by 1 late arterial sample ($APTAC_{1sample}$) and the individual IDIF ($APTAC_{IDIF}$) were compared to the gold standard of serial arterial sampling ($APTAC_{sampled}$) using the area under the curve (AUC). Additionally, these three methods of APTAC determination were evaluated with Patlak MR_{glc} estimation and with ΔMR_{glc} for therapy effects using serial sampling as gold standard. **Results:** Excellent individual fits to the function were derived with significantly different decay constants ($p<0.001$). Correlations between AUC from $APTAC_{AA/iDV}$, $APTAC_{1sample}$ and $APTAC_{IDIF}$ with the gold standard ($APTAC_{sampled}$) were 0.880, 0.994 and 0.856 respectively. For MR_{glc} these correlations were 0.963, 0.994 and 0.966 respectively.

In response monitoring these correlations were 0.947, 0.982 and 0.949 respectively. Additional scaling by one late arterial sample showed a significant improvement ($p<0.001$). **Conclusion:** The fitted input function calibrated for AA and iDV had similar performance as an IDIF. Using one late arterial sample, this improved significantly. The proposed model can be used where an IDIF is not available or when serial arterial sampling is not feasible.

Keywords: [^{18}F]FDG – Positron emission tomography – Chemotherapy – Therapy Monitoring – Input Function – Theoretical Models – Pharmacokinetics – Body Fluid Compartments – Least-Squares Analysis – Tissue Distribution

Introduction

Pharmacokinetic analysis of [^{18}F]-2-fluoro-2-deoxy-D-glucose (^{18}F-FDG) by dynamic positron emission tomography (PET) requires both the arterial plasma time activity concentration curve (APTAC, $C_p(t)$ or input function) and the tissue time activity curve measured by PET (TTAC or $C_T(t)$) to be available to create a Patlak plot (*1*) ($C_T(t)/C_p(t)$ versus $\int_0^t C_p(\tau)d\tau/C_p(t)$), from which the glucose metabolic rate (MR_{glc}) in the tissue of interest can be derived. Special interest in this type of quantitative analysis has risen for oncological patients for prognostic stratification and response monitoring of disease.

The gold standard to obtain the APTAC is by measuring decay-corrected activity concentrations in plasma obtained by serial arterial sampling (*2*). This is an invasive and potentially harmful procedure for the patient and exposes the personnel to radiation. Complications attributed to radial artery cannulation include temporary occlusion (19.7%) and hematoma formation (14.4%), local infection (0.72%), sepsis (0.13%), permanent occlusion (0.09%) and pseudo-aneurysm (0.09%) (*3*), some of which require medical intervention. Therefore, different methods have been developed to reduce these drawbacks. The major four alternatives to serial arterial sampling are: (arterialized) venous blood sampling (*4, 5*), estimation of image-derived input functions (IDIF) (*6-12*), modeling a population-based input function (*13-17*) and extraction of whole blood input functions using sophisticated mathematical image segmentation methods (i.e. cluster analysis (*18*) and independent component analysis (*19-21*)).

A drawback of venous sampling is the time-dependent ratio of ^{18}F-FDG in venous to arterial blood (0.61-0.88, 5-50 min post-injection) (*4, 5*). Therefore, shunting of arterial blood to the venous system (the "heated hand" procedure) is used to improve these ratios to 0.92-1.05 (*4*). This arterialized venous sampling technique still requires cannulation of an extra vein, and exposes personnel to radiation.

IDIFs require a large blood pool (aorta, left ventricle) within the field-of-view of the PET-image. IDIFs show systematic error, since activity concentration is measured in whole blood, which is known to be lower than in plasma (ratio ~0.925-0.95) (*6-8*). Moreover, partial volume effects cause inaccuracy by spill-over of activity from or to the surrounding tissues (e.g. myocardium) (*6, 9*). Finally, additional noise is introduced due to the limited number of counts in the short early time frames. Since underestimation due to spill-out of the IDIF activity concentration values leads to overestimation of MR_{glc} and overestimation due to spill-in of surrounding IDIF activity concentration values (in later time frames) leads to underestimation of MR_{glc} (*6, 9*), correction is necessary (*10-12*).

A population-based APTAC is based on averaging of normalized sampled blood data of multiple patients. Several corrections were introduced, based on administered activity (AA), bodyweight and blood transit time (*13*) or AA and body surface area (*14, 15*). The latter provided a reliable estimation of MR_{glc}, but yielded less accurate parameter values in pharmacokinetic analysis. Another method is "fitting" of the sampled data to an equation assuming the ^{18}F-FDG distribution in the vascular system as a compartment model on its own (*16, 17, 22*).

Here, we describe an APTAC model that is based on fitting of a large series of arterially sampled oncological patients to a mathematical equation (*16, 17, 22*). The model APTAC was calibrated to individual patients of a separate patient population by either an estimation of the distribution volume of FDG (*14, 15*) or one late arterial blood sample and compared to the gold standard of arterial sampling and the IDIF. The performance of both models was assessed by comparison of the APTACs themselves and by their influence on Patlak MR_{glc} and therapy response (ΔMR_{glc}) evaluation.

Patients & methods

1. Patient population, arterial sampling procedure

Data of 120 dynamic ^{18}F-FDG-PET scans with serial arterial sampling data were re-analyzed. Scans were randomly distributed over two groups (table 1), a parameter-identification group (n=80) and a parameter-validation group (n=40). For latter group, both a pre-treatment and a follow-up scan, after 2-3 courses of chemotherapy, was included. The details of ^{18}F-FDG-PET and arterial plasma data acquisition are described elsewhere (*9*) with the only difference that they were reconstructed using OSEM (ordered subsets expectation maximization) with 4 iterations and 16 subsets with a Gauss filter of 5 mm in all directions. In short, fasted normoglycemic patients were injected with ^{18}F-FDG by an automated standardized infusion protocol. Directly thereafter, 17 arterial blood samples were taken at set time points from which plasma was obtained by centrifugation to provide a sampled arterial plasma time activity concentration curve ($APTAC_{sampled}$). Simultaneously, dynamic PET-acquisition, consisting of 16 timeframes of variable length, was obtained to provide both the tissue (TTAC) and the image-derived blood time activity concentration curves ($APTAC_{IDIF}$).

2. Parameter-identification study (n=80)

2.1 Normalization of the $APTAC_{sampled}$

The initial plasma concentration of ^{18}F-FDG (C_p*(0), [$MBq \cdot L^{-1}$]), was used to normalize the $APTAC_{sampled}$. It was defined as the expected ^{18}F-FDG concentration directly after tracer injection, assuming instant homogenization and is dependent on the administered activity (AA, [MBq]) and the (apparent) initial distribution volume (iDV, [L]) (*14, 15*). To avoid confusion, an '*' is added, since the sampled activity concentration at t=0 is 0 $MBq \cdot L^{-1}$.

In the period between 5 and 30 min post-injection, the plasma and extravascular extracellular ^{18}F-FDG pool of the whole body were assumed to be in equilibrium (*23*). Before this period, the tracer is being distributed over the body and in the period thereafter, the tracer is mainly being metabolized and excreted. Within this interval we sampled four times (7.5, 12.5, 17.5 and 25 minutes post-injection) (*9*), therefore to obtain $C_p^*(0)$, semilogarithmic recordings of these four points were linearly extrapolated back to t=0 (y-intercept) (*15, 23*).

2.2 Estimation of iDV by bodyweight and height

By definition, the iDV represents the (virtual) volume of the plasma and extravascular extracellular ^{18}F-FDG pool. The iDV can be estimated by (*14, 15*):

$$iDV = \frac{\mathrm{AA}}{\mathrm{C_p^*(0)}} = c \cdot \mathrm{H^h} \cdot W^w \qquad \text{Eq. 1}$$

where H is patient height [m] and W is patient bodyweight [kg]. Iteratively h, w and c were derived for which the coefficient of variation of c ($CV_c = \frac{standard\ deviation_c}{mean_c}$) is smallest in the parameter-identification data.

2.3 Fitting of the normalized $APTAC_{sampled}$

Using the three-compartment model for the blood pool as proposed by Feng *et al.*(*16*), simplified by Eberl *et al.*(*17*), the normalized $\mathrm{APTAC_{sampled}}$ can be approximated by:

$$\frac{APTAC_{sampled}(\mathrm{t})}{C_p^*(0)} = \begin{cases} 0 & t < -\frac{b}{a} \\ a \cdot t + b & -\frac{b}{a} \le t < \tau \\ \sum_{i=1}^{3} A_i \cdot e^{-\lambda_i \cdot (t-\tau)} & t \ge \tau \end{cases} \qquad \text{Eq. 2}$$

where τ is the time to peak activity concentration. The normalized sampled plasma curves were fitted by linear curve fitting ($t<\tau$) and by nonlinear least squares ($t\geq\tau$) to obtain the eight free parameters in every patient of the parameter-identification study. Since

chemotherapy might influence ^{18}F-FDG distribution and clearance, the parameter values were compared between scans made in patients who did and did not receive chemotherapy.

3. Parameter-validation study (n=40)

3.1 Image derived input function and tumor time-activity curves

The $APTAC_{IDIF}$ was determined in manually placed volumes of interest (VOIs) over the ascending aorta (thoracic images) or descending aorta (abdominal images), known to correlate best with the gold standard (*9*) on summed images of the period 30-90 sec post-injection. The TTAC was obtained semi-automatically by placing VOIs in the summed images of the period 20-50 min post-injection over the largest lesion, fully present in the field of view, using a threshold of 50% of its maximum voxel value. All image analysis was performed using the Inveon Research Workplace (IRW version 2.2, Siemens, Knoxville, TN, USA).

3.2 Comparison of calibrated plasma time activity curves and glucose metabolic rates

Median values of APTAC-parameters derived from the parameter-identification study were used for the population-based APTAC which was calibrated to each individual patient, using two methods: by multiplication by either AA [MBq] divided by iDV [L] (estimated using equation 1), further mentioned as $APTAC_{AA/iDV}$ or by the plasma activity concentration of one late arterial sample ($APTAC_{1sample}$).

The performance of the three curves ($APTAC_{AA/iDV}$, $APTAC_{1sample}$ and $APTAC_{IDIF}$) was compared to that of the gold standard ($APTAC_{sampled}$) by their area under the curve (AUC), determined by trapezoid integration.

MR_{glc} was determined using all four plasma input curves by Patlak graphical analysis (*1*). In the Patlak approximation, the lumped constant, accounting for the difference in

glucose and ^{18}F-FDG affinity was set to 1 and the tumor blood fraction was set to 0, therefore the slope of the Patlak plot was K_i and the intercept was $\frac{K_1 \cdot k_2}{(k_2 + k_3)^2}$. MR_{glc} can then be determined by multiplying the linear regression (5-50 min post-injection) by the plasma glucose concentration.

4. Statistical analysis

All variables were assessed for normality (Shapiro-Wilk, skewness and kurtosis) and are either displayed as mean (± standard deviation) or median (interquartile range, IQR). Comparison between two independent groups was performed by the t-test, the Mann-Whitney U-test or χ^2 test. Comparison of λ_1-λ_3 was performed by Friedman's analysis of variance (ANOVA). Correlations between the AUC, MR_{glc} and ΔMR_{glc} of the different curves compared to the gold standard were assessed by Pearson's r or Spearman's ρ and linear regression and are displayed as Bland-Altman plots. Confidence intervals for correlation coefficients were compared after Fisher's z transformation (*24*). Analysis was performed by SPSS 16.0.2. Two-sided significance was set at the 0.050 level.

RESULTS

1. Parameter-identification study

A median iDV of 12.7 L (corresponding to 0.1683 L per kg bodyweight) was calculated. Iterative determination of the function to estimate the iDV led to h=1.257, w=0.582 and c=0.533 $L \cdot m^{-1.257} \cdot kg^{-0.582}$ (minimum CV_c=0.171, adjusted R^2=0.3181).

Fitting of the 80 $APTAC_{sampled}$ by equation 2 led to a minimum adjusted R^2 of 0.8533, 80% of fits had an adjusted R^2 > 0.9500. Resulting parameters for the normalized $APTAC_{sampled}$ are provided in table 2. No significant difference in ^{18}F-FDG-clearance could

be detected ($p>0.326$) between patients that did and did not receive chemotherapy. The three decay constants (λ_1-λ_3) were significantly different ($p<0.001$, figure 1).

2. Parameter-validation study

The correlation between the AUC of the $APTAC_{AA/iDV}$ and $APTAC_{sampled}$ was 0.880. Using one arterial sample for calibration, this improved to 0.994 ($p<0.001$). The mean AUC of $APTAC_{AA/iDV}$ was similar (462 ± 119 $MBq \cdot L^{-1} \cdot min$) and of $APTAC_{1sample}$ slightly lower (468 ±107 $MBq \cdot L^{-1} \cdot min$) than the gold standard ($APTAC_{sampled}$: 475 ± 108 $MBq \cdot L^{-1} \cdot min$, $p=0.156$ and $p<0.001$ respectively). The $APTAC_{IDIF}$ showed much lower AUCs than $APTAC_{sampled}$ (392 ± 99 $MBq \cdot L^{-1} \cdot min$, $p<0.001$) with a correlation coefficient between these parameters of 0.856.

Comparison between MR_{glc} is shown in figure 2 (left panels). Adding one arterial sample (25 min post-injection) improved correlation between MR_{glc} determined by $APTAC_{AA/iDV}$ and $APTAC_{sampled}$ from $\rho=0.963$ to $\rho=0.994$ ($p<0.001$). MR_{glc} determined by IDIF was significantly higher than the gold standard; correlation was similar to that of $APTAC_{AA/iDV}$ ($\rho=0.966$).

Comparison between therapy effects (ΔMR_{glc}) is shown in figure 2 (right panels). Adding one arterial sample (25 min post-injection) improved correlation between ΔMR_{glc} determined by $APTAC_{AA/iDV}$ and $APTAC_{sampled}$ from $\rho=0.947$ to $\rho=0.982$ ($p=0.012$). ΔMR_{glc} determined by $APTAC_{IDIF}$ had similar correlation to the gold standard as $APTAC_{AA/iDV}$ ($\rho=0.949$).

Any arterial sample taken after 7.5 min post-injection showed similar high correlations when comparing MR_{glc} ($\rho \geq 0.9916$) or ΔMR_{glc} ($\rho \geq 0.9759$) measured by $APTAC_{sampled}$ and $APTAC_{1sample}$.

Discussion

This study describes the performance of a population-based APTAC based on fitting patient data to a mathematical equation on Patlak determination of MR_{glc} and on chemotherapy response evaluation. Its accuracy is comparable to that of an IDIF, explaining 93% of variance in MR_{glc} (90% in response evaluation by ΔMR_{glc}), but addition of one late arterial sample improves this to 99% (96% in response evaluation by ΔMR_{glc}). Where the IDIF is fully individual, the proposed method is a population average, calibrated to individual patient parameters without the need for serial arterial sampling. It can be used when scanning body regions where blood-pools are unavailable, such as the extremities. The model can be further improved by including one arterial sample. It can be expected that a late arterialized venous sample might adequately replace the arterial sample, since more than ~30 min after ^{18}F-FDG injection, activity concentrations of arterial and arterialized venous blood are highly similar (*4, 5*). This sample might also be used to obtain an accurate measurement of the plasma glucose level, as long as radiation safety regulations do not prohibit this analysis in the clinical chemistry laboratory. As shown, MR_{glc} was significantly overestimated using an IDIF compared to the gold standard. Both the partial-volume effect and the fact that whole blood activity concentrations are lower than in plasma cause underestimation of the (integral of the) APTAC. From the Patlak-equation it can be derived that an underestimation of the APTAC as well as its integral, cause overestimation of the MR_{glc}. The quality of the IDIF can be improved by correction for the partial-volume and spill-over effects (*25*). Moreover, correction for the activity concentrations in whole blood to plasma concentrations can be performed using correction by hematocrit (*19*) or modeled erythrocyte uptake (*26*). In addition the noise in the short early time frames contribute to its inaccuracy. Recently eight methods for the estimation of the carotid IDIF in human brain studies were compared to the reference input function (arterially sampled) with respect to cerebral MR_{glc} and individual rate constants in a study consisting of

phantoms and healthy volunteers. The authors concluded that blood-sample-free methods provided less reliable results as compared with those obtained using the methods that require the use of blood samples, even when limited to a single sample (*27*). Therefore, calibration of our IDIFs by one late venous sample would probably have improved its accuracy. The advantage of a more patient-specific rather than a generic input function is especially of importance for pharmacokinetic analysis, since the exact shape of the APTAC in the artery feeding the tumor is vital and is usually different from a remote artery (due to delay and dispersion by the intra-individual variation in the impulse-response characteristics of the vascular system).

One method of calibration of the population-based curve was by the method of Sadato *et al.*(*23*) (AA/iDV). They report a mean iDV scaled to bodyweight (iDV_{BW}) of 0.1627 $L \cdot kg^{-1}$ similar to this study (median iDV_{BW} of 0.1683 $L \cdot kg^{-1}$). Around 50%-60% of the bodyweight of an average adult is water, of which 25%-45% (0.18 $L \cdot kg^{-1}$) is extracellular fluid (the volume of water in which ^{18}F-FDG dissolves), stressing both the concordance and plausibility of this result (*28*). We used the function of Shiozaki *et al.* (*15*) to fit the iDV. They reported: $iDV[mL]=39.0 \cdot H[cm]^{0.80} \cdot W[kg]^{0.35}$. This appears different from the present study ($iDV[L]=0.533 \cdot H[m]^{1.257} \cdot W[kg]^{0.582}$), but they were only slightly off our optimum (CV_c=0.18 versus CV_c=0.17). A dissimilar distribution of body habitus in their (Asian) population might causative for this difference.

As shown in figure 2, the difference between MR_{glc} calculated by $APTAC_{1sample}$ and $APTAC_{sampled}$ was small, therefore the net influx constant determined by Patlak analysis was accurate. For determination of the individual rate-constants however, the inaccuracy will probably be much higher. For Patlak analysis, only the integral of the APTAC and the late (>5 min) activity concentrations of the arterial plasma are of relevance, but for the accurate estimation of the individual rate constants of glucose pharmacokinetics, the exact shape of the APTAC is vital, due to both the function (including a convolution operation) and the method for parameter estimation (non-linear least squares). The delay and

dispersion between the APTAC in the artery feeding the tissue of interest and a remote artery, is of major importance for the accurate determination of the fast rate constants (K_1 and k_2) and blood fraction (V_b). Moreover, the use of a generic input function for pharmacokinetic analysis should be considered because of the large intra-individual variation of the slow clearance rate constants of ^{18}F-FDG (λ_3 (and in lesser extent in λ_2) in figure 1 and table 2). The assumption of a single clearance profile for all patients might therefore lead to inaccurate estimation of the slower rate constants (k_3 and (if exists) k_4) of individual patients.

The proposed model therefore should be evaluated further for purpose of microparameter estimation before implementation. This, however, was out of the scope of this study.

None of the previously published articles on population-based input curve used an IDIF for comparison and most studies consist of small series of non-oncological patients, but reproducibility is high (table 3). The studies that used tri-exponential clearance of ^{18}F-FDG as function for the APTAC (*16, 17, 22*) found similar decay as this study (figure 3). The results shown in figure 1 suggest a high (linear) correlation between A_3 and λ_3. This suggests that the model might be simplified omitting one parameter. We did not verify this in this study.

Conclusion

The current model of the APTAC of ^{18}F-FDG, calibrated by one late arterial sample shows high accuracy for Patlak MR_{glc} calculation and treatment response monitoring. It allows dynamic scanning of areas without large vessels in the FOV, such as the extremities, is less invasive and causes less radiation exposure to personnel than arterial sampling. Even

without a calibrating sample available, this model has the same accuracy as an IDIF without its inherent disadvantages.

Figures

Figure 1: Scatter plot of $\log_{10}(A_j)$ versus $\log_{10}(\lambda_j)$, showing clustering of the three decay constants.

Figure 2: Bland-Altman plots of comparison between any of the three evaluated APTACs and the gold standard. In the Bland-Altman plots the mean difference is displayed by the solid line and the 95% confidence interval (95CI) by the dotted lines. Unstandardized regression coefficients are displayed with corresponding 95CI. 1# sample: calibrated by one arterial sample at 25 min post injection; AA/iDV: calibrated by administered activity and initial distribution volume, APTAC: arterial plasma time activity concentration curve, IDIF: image derived input function, MR_{glc}: glucose metabolic rate.

Figure 3: Comparison of tri-exponential ^{18}F-FDG-clearance in our study and 3 previous publications (*16, 17, 22*). Functions were normalized to the total area under the curve. Dif.: absolute differences of our clearance curve compared to the three found in literature.

Tables

Table 1: Comparison between parameter-identification and parameter-validation group with statistical significance of group difference.

	Identification	Validation	p
PET scans (individual patients)	80 (49)	40 (20)	0.327*
Male sex [% of scans]	60	70	0.320*
Median age (range) [years]	60.7 (44.8; 78.9)	60.1 (44.7; 71.9)	0.225†
Mean administered activity (SD) [MBq]	207 (40.1)	200 (35.8)	0.314‡
Median plasma glucose concentration (range) [mmol·L^{-1}]	5.3 (4.2; 10.0)	5.3 (4.2; 8.3)	0.125†
Median BMI (range) [kg·m^{-2}]	25.8 (22.7; 27.4)	25.9 (19.8; 33.7)	0.508†
Cancer localization [% of scans]			
Lung (non-small cell)	50	50	
Colorectal	45	40	
Breast	5	10	0.618*

BMI: body mass index, PET: positron emission tomography. SD: standard deviation. *χ^2 test, †Mann-Whitney U test, ‡independent samples t-test

Table 2: Results of fitting of the normalized plasma data of the parameter-identification group and subgroup analysis between pre-therapy scans and post-therapy scans.

Parameter	All scans (n=80) Median	[IQR]	Pre-therapy scans (n=40) Median	[IQR]	Follow-up scans (n=40) Median	[IQR]	p*
τ [min]	1.25	[1.25; 1.50]	1.25	[1.25; 1.25]	1.25	[1.25; 1.50]	0.077
a [min^{-1}]	4.911	[4.188; 5.709]	4.914	[4.154; 5.660]	4.911	[4.203; 5.771]	0.672
b	-2.077	[-2.817; -1.321]	-1.195	[-2.805; -1.096]	-2.225	[-2.961; -1.503]	0.168
A_1	2.785	[2.302; 3.212]	2.718	[2.241; 3.152]	2.937	[2.321; 3.300]	0.326
λ_1 [min^{-1}]	6.133	[4.646; 8.114]	6.034	[4.121; 8.064]	6.133	[4.833; 8.322]	0.622
A_2	0.7085	[0.6492; 0.8011]	0.6966	[0.6340; 0.8434]	0.7229	[0.6694; 0.8130]	0.589
λ_2 [min^{-1}]	0.2541	[0.2075; 0.3071]	0.2400	[0.1881; 0.3423]	0.2592	[0.2285; 0.2847]	0.805
A_3	0.7721	[0.7177; 0.8070]	0.7699	[0.6861; 0.8286]	0.7741	[0.7385; 0.7970]	0.920
λ_3 [min^{-1}]	0.01443	[0.01248; 0.01595]	0.01446	[0.01206; 0.01656]	0.01434	[0.01260; 0.01590]	0.562

IQR: interquartile range; *Mann-Whitney U-test.

Table 3: Literature review of publication on population-based APTACs and IDIFs.

Reference	n	Method	Calibration	AUC	MR_{glc}
Takikawa (*13*)	10 / 24	Arithmetic mean	2 arterial 1 AVS	0.998 0.998	0.992 0.989
Tsuchida (*14*)	44 / 10	Arithmetic mean	-	+3.5%±2.2%	+2.9%±1.9%
Shiozaki (*15*)	101 / 192	Arithmetic mean	AA/iDV	+7.2%±5.7%	+8.9%±7.3%
Bentourkia (*29*)	20 / same 20	Fit to equation	-	-	0.998
Eberl (*17*)	26 / 26	Fit to equation	2 AVS	-	0.995
de Geus-Oei (*9*)	136	IDIF	-	-	0.98
This study	80 / 40	Fit to equation	AA/iDV 1 arterial	0.880 0.994	0.963 0.994
		IDIF	-	0.856	0.966

AA/iDV: administered activity/initial distribution volume of ^{18}F-FDG; APTAC: arterial plasma time activity concentration curve; AUC: correlation or mean % difference between area under the curve of population-based curve and serial arterial sampling; AVS: arterialized venous samples; IDIF: image-derived input function; MR_{glc}: correlation or mean % difference between glucose metabolic rate of population-based curve and serial arterial sampling; n: number of patients (to derive curve / to validate curve).

References

1. Patlak CS, Blasberg RG, Fenstermacher JD. Graphical evaluation of blood-to-brain transfer constants from multiple-time uptake data. *J Cereb Blood Flow Metab.* 1983;3:1-7.

2. Greuter HN, Boellaard R, van Lingen A, Franssen EJ, Lammertsma AA. Measurement of 18F-FDG concentrations in blood samples: comparison of direct calibration and standard solution methods. *Journal of nuclear medicine technology.* 2003;31:206-209.

3. Scheer B, Perel A, Pfeiffer UJ. Clinical review: complications and risk factors of peripheral arterial catheters used for haemodynamic monitoring in anaesthesia and intensive care medicine. *Critical care (London, England).* 2002;6:199-204.

4. van der Weerdt AP, Klein LJ, Visser CA, Visser FC, Lammertsma AA. Use of arterialised venous instead of arterial blood for measurement of myocardial glucose metabolism during euglycaemic-hyperinsulinaemic clamping. *Eur J Nucl Med Mol Imaging.* 2002;29:663-669.

5. Wakita K, Imahori Y, Ido T, et al. Simplification for measuring input function of FDG PET: investigation of 1-point blood sampling method. *J Nucl Med.* 2000;41:1484-1490.

6. van der Weerdt AP, Klein LJ, Boellaard R, Visser CA, Visser FC, Lammertsma AA. Image-derived input functions for determination of MRGlu in cardiac (18)F-FDG PET scans. *J Nucl Med.* 2001;42:1622-1629.

7. Dhawan V, Takikawa S, Robeson W, et al. Quantitative brain FDG/PET studies using dynamic aortic imaging. *Phys Med Biol.* 1994;39:1475-1487.

8. Ohtake T, Kosaka N, Watanabe T, et al. Noninvasive method to obtain input function for measuring tissue glucose utilization of thoracic and abdominal organs. *J Nucl Med.* 1991;32:1432-1438.

9. de Geus-Oei LF, Visser EP, Krabbe PF, et al. Comparison of image-derived and arterial input functions for estimating the rate of glucose metabolism in therapy-monitoring 18F-FDG PET studies. *J Nucl Med.* 2006;47:945-949.

10. Lin KP, Huang SC, Choi Y, Brunken RC, Schelbert HR, Phelps ME. Correction of spillover radioactivities for estimation of the blood time-activity curve from the imaged LV chamber in cardiac dynamic FDG PET studies. *Phys Med Biol.* 1995;40:629-642.

11. Gambhir SS, Schwaiger M, Huang SC, et al. Simple noninvasive quantification method for measuring myocardial glucose utilization in humans employing positron emission tomography and fluorine-18 deoxyglucose. *J Nucl Med.* 1989;30:359-366.

12. Chen K, Bandy D, Reiman E, et al. Noninvasive quantification of the cerebral metabolic rate for glucose using positron emission tomography, 18F-fluoro-2-deoxyglucose, the Patlak method, and an image-derived input function. *J Cereb Blood Flow Metab.* 1998;18:716-723.

13. Takikawa S, Dhawan V, Spetsieris P, et al. Noninvasive quantitative fluorodeoxyglucose PET studies with an estimated input function derived from a population-based arterial blood curve. *Radiology.* 1993;188:131-136.

14. Tsuchida T, Sadato N, Yonekura Y, et al. Noninvasive measurement of cerebral metabolic rate of glucose using standardized input function. *J Nucl Med.* 1999;40:1441-1445.

15. Shiozaki T, Sadato N, Senda M, et al. Noninvasive estimation of FDG input function for quantification of cerebral metabolic rate of glucose: optimization and multicenter evaluation. *J Nucl Med.* 2000;41:1612-1618.

16. Feng D, Huang SC, Wang X. Models for computer simulation studies of input functions for tracer kinetic modeling with positron emission tomography. *Int J Biomed Comput.* 1993;32:95-110.

17. Eberl S, Anayat AR, Fulton RR, Hooper PK, Fulham MJ. Evaluation of two population-based input functions for quantitative neurological FDG PET studies. *Eur J Nucl Med.* 1997;24:299-304.

18. Liptrot M, Adams KH, Martiny L, et al. Cluster analysis in kinetic modelling of the brain: a noninvasive alternative to arterial sampling. *Neuroimage.* 2004;21:483-493.

19. Su KH, Wu LC, Liu RS, Wang SJ, Chen JC. Quantification method in [18F]fluorodeoxyglucose brain positron emission tomography using independent component analysis. *Nucl Med Commun.* 2005;26:995-1004.

20. Naganawa M, Kimura Y, Ishii K, Oda K, Ishiwata K, Matani A. Extraction of a plasma time-activity curve from dynamic brain PET images based on independent component analysis. *IEEE Trans Biomed Eng.* 2005;52:201-210.

21. Chen K, Chen X, Renaut R, et al. Characterization of the image-derived carotid artery input function using independent component analysis for the quantitation of [18F] fluorodeoxyglucose positron emission tomography images. *Phys Med Biol.* 2007;52:7055-7071.

22. Hunter GJ, Hamberg LM, Alpert NM, Choi NC, Fischman AJ. Simplified measurement of deoxyglucose utilization rate. *J Nucl Med.* 1996;37:950-955.

23. Sadato N, Tsuchida T, Nakaumra S, et al. Non-invasive estimation of the net influx constant using the standardized uptake value for quantification of FDG uptake of tumours. *Eur J Nucl Med.* 1998;25:559-564.

24. Fisher RA. On the 'probable error' of a coefficient of correlation deduced from a small sample. *Metron* 1921;1:3-32.

25. Fang YH, Muzic RF, Jr. Spillover and partial-volume correction for image-derived input functions for small-animal 18F-FDG PET studies. *J Nucl Med.* 2008;49:606-614.

26. Lee JS, Su KH, Lin JC, et al. A novel blood-cell-two-compartment model for transferring a whole blood time activity curve to plasma in rodents. *Comput Methods Programs Biomed.* 2008;92:299-304.

27. Zanotti-Fregonara P, Fadaili EM, Maroy R, et al. Comparison of eight methods for the estimation of the image-derived input function in dynamic [(18)F]-FDG PET human brain studies. *J Cereb Blood Flow Metab.* 2009.

28. Singer GG, Brenner BM. Fluid and Electrolyte Disturbances. In: Fauci AS, Braunwald E, Kasper DL, et al., eds. *Harrison's Principles of Internal Medicine, 17th Edition.* Vol 1: McGraw-Hill Education - Europe 2008:274-285.

29. Bentourkia M, Bol A, Ivanoiu A, et al. A standardized blood sampling scheme in quantitative FDG-PET studies. *IEEE Trans Med Imaging.* 1999;18:379-384.

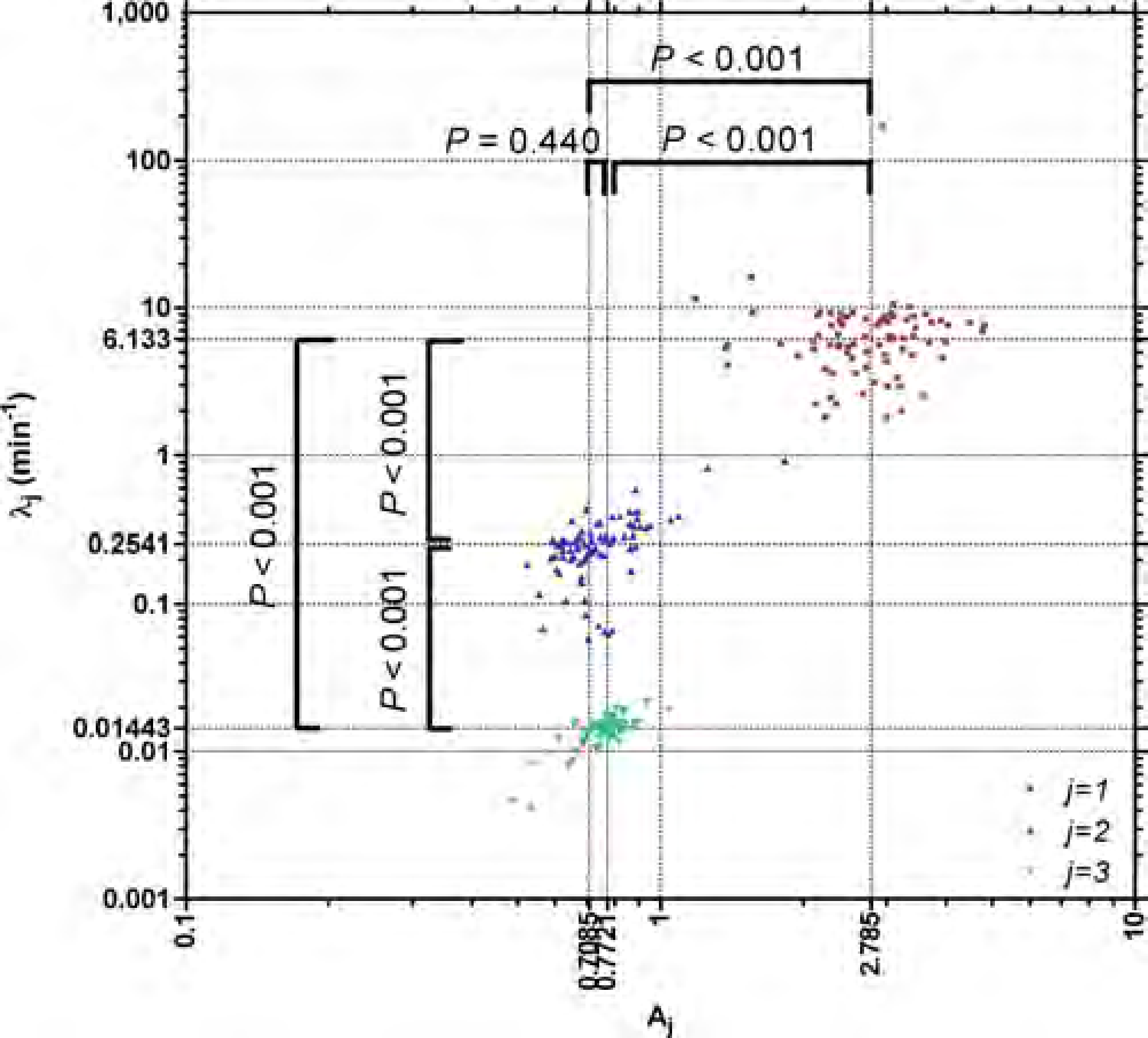
1,000
100
10
6.133
1
0.2541
0.1
0.01443
0.01
0.001
λ_j (min^{-1})
P < 0.001
P = 0.440
P < 0.001
P < 0.001
P < 0.001
P < 0.001
j=1
j=2
j=3
0.1
0.47085
0.77921
1
2.785
10
A_j

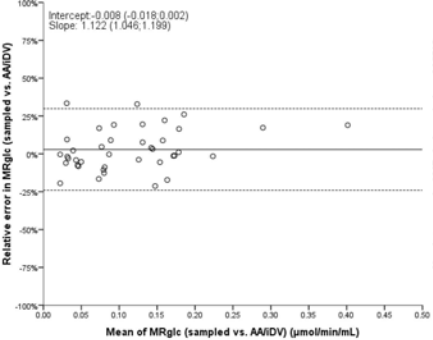
Intercept:-0.008 (-0.018;0.002)
Slope: 1.122 (1.046;1.199)
Relative error in MRglc (sampled vs. AA/iDV)
Mean of MRglc (sampled vs. AA/iDV) (µmol/min/mL)

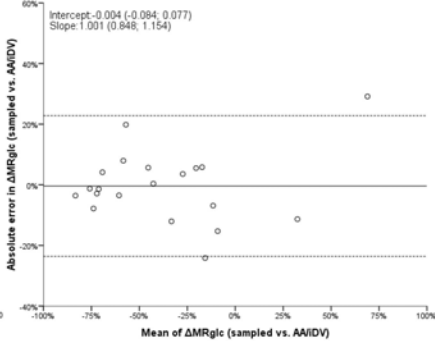
Intercept:-0.004 (-0.084; 0.077)
Slope:1.001 (0.848; 1.154)
Absolute error in ΔMRglc (sampled vs. AA/iDV)
Mean of ΔMRglc (sampled vs. AA/iDV)

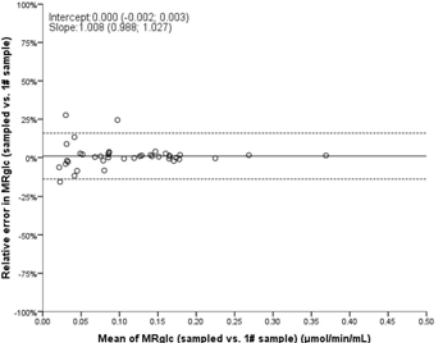
Intercept:0.000 (-0.002; 0.003)
Slope:1.008 (0.988; 1.027)
Relative error in MRglc (sampled vs. 1# sample)
Mean of MRglc (sampled vs. 1# sample) (µmol/min/mL)

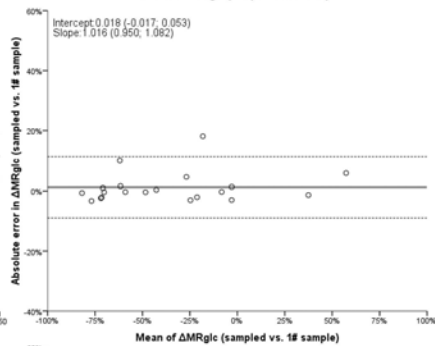
Intercept:0.018 (-0.017; 0.053)
Slope:1.016 (0.950; 1.082)
Absolute error in ΔMRglc (sampled vs. 1# sample)
Mean of ΔMRglc (sampled vs. 1# sample)

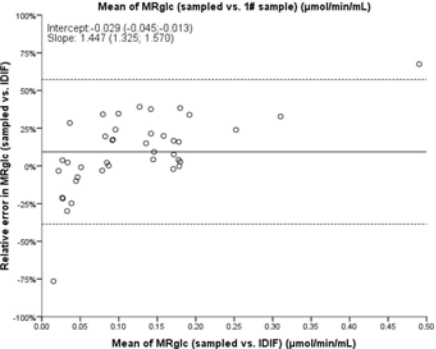
Intercept:-0.029 (-0.045;-0.013)
Slope: 1.447 (1.325; 1.570)
Relative error in MRglc (sampled vs. IDIF)
Mean of MRglc (sampled vs. IDIF) (µmol/min/mL)

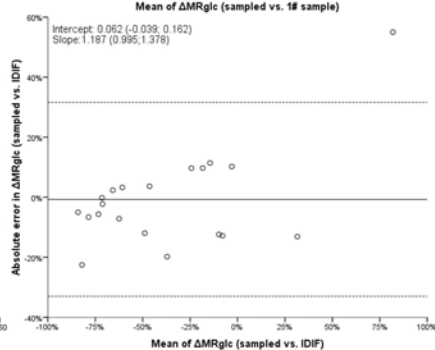
Intercept: 0.062 (-0.039; 0.162)
Slope:1.187 (0.995;1.378)
Absolute error in ΔMRglc (sampled vs. IDIF)
Mean of ΔMRglc (sampled vs. IDIF)

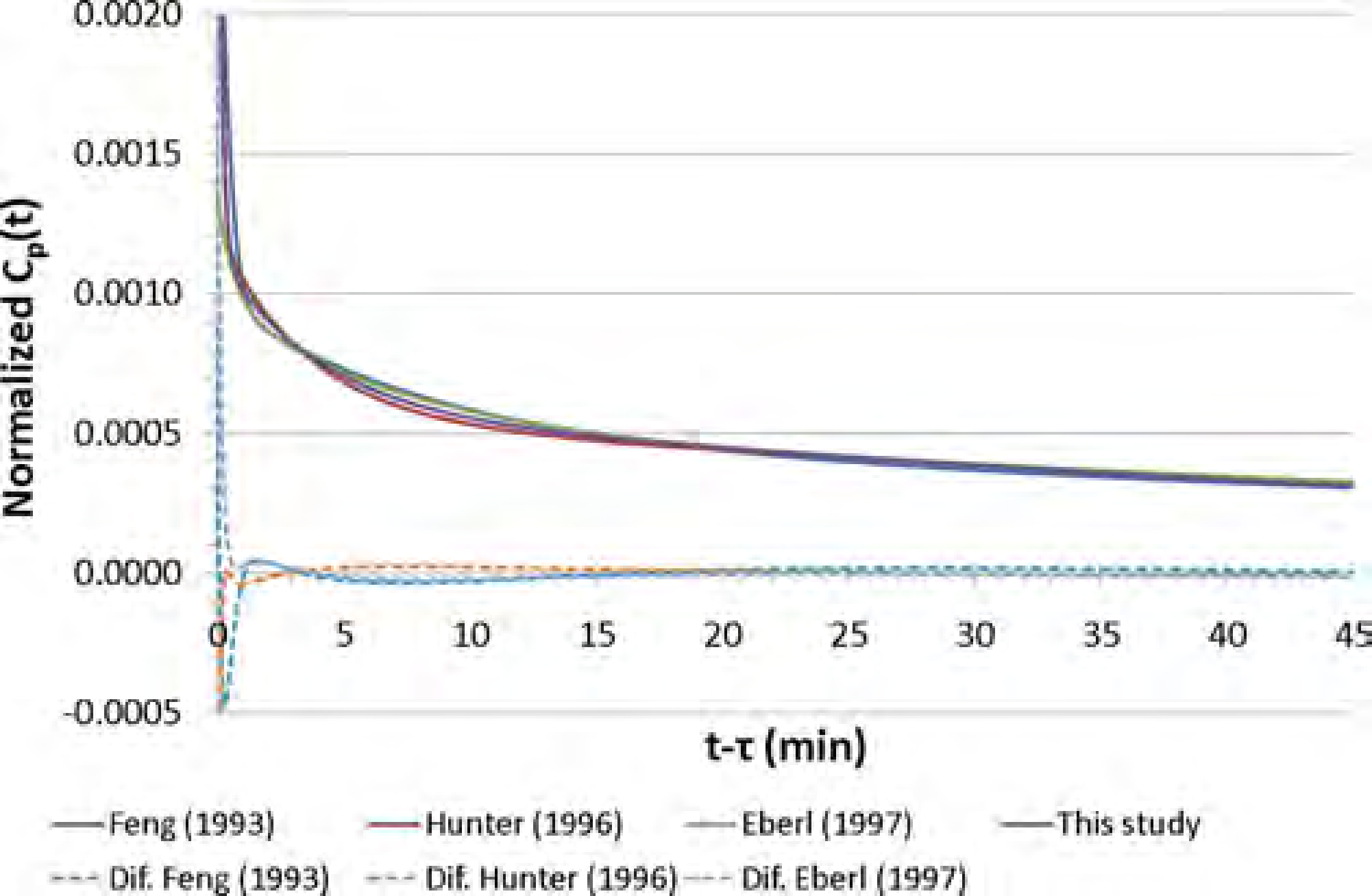
0.0020
0.0015
0.0010
0.0005
0.0000
-0.0005
Normalized $C_p(t)$
0
5
10
15
20
25
30
35
40
45
t-τ (min)
Feng (1993)
Hunter (1996)
Eberl (1997)
This study
Dif. Feng (1993)
Dif. Hunter (1996)
Dif. Eberl (1997)